JOURNAL OF GEOPHYSICAL RESEARCH, VOL. 115, C07008, doi:10.1029/2009JC005834, 2010

Identification of typical scenarios for the surface Lagrangian residual circulation in the Iroise Sea

Héloïse Muller,[1,2,3] Bruno Blanke,[2] Franck Dumas,[3] and Vincent Mariette[1]

Received 23 September 2009; revised 11 January 2010; accepted 10 February 2010; published 13 July 2010.

[1] This paper describes the surface Lagrangian residual circulation (LRC) over 2.5 day intervals in the Iroise Sea, west of France, and evaluates, for operational purposes, the influence of the different physical mechanisms that govern it. The method consists of the calculation of water displacements with a diagnostic Lagrangian tool that computes the trajectories of numerical particles in a given velocity field. The LRC is inferred from trajectories integrated over five M2 tidal cycles. The analysis is applied to both gridded genuine current measurements and ocean model outputs: the sea surface currents are derived from high-frequency (HF) radar measurements and from MARS, a 3-D regional ocean model used here in idealized configurations. To substantiate the analysis, the Lagrangian residual currents are also compared to genuine movements of drifters released in the Iroise Sea in 2005 and 2007. The LRC is mapped for typical scenarios identified from the Lagrangian analysis of HF radar surface currents measured in winter and summer, under weak (<7 m/s) and strong (>10 m/s) wind conditions, and in neap tide and spring tide seasons. Idealized numerical simulations that switch on and off each individual physical process are used to isolate in the LRC the patterns induced by the atmospheric forcing, tides, and density-driven currents.

Citation: Muller, H., B. Blanke, F. Dumas, and V. Mariette (2010), Identification of typical scenarios for the surface Lagrangian residual circulation in the Iroise Sea, *J. Geophys. Res.*, *115*, C07008, doi:10.1029/2009JC005834.

1. Introduction

[2] The Iroise Sea (Figure 1), west of France, is a particularly complex and interesting area in terms of hydrodynamics, thermodynamics, biological activities, and maritime traffic. Three physical processes have a major influence on the velocity and thermohaline structure: a semidiurnal tide, the meteorological forcing, and strong thermal gradients in summer. The interactions between the barotropic tide, irregularities of the coastline, and bathymetry imply currents up to 4 m/s at spring tide nearby the islands and capes of this shallow area (110 m on average) [*Le Duff and Hily*, 1999]. The Iroise Sea is also subject to the swell, waves, and currents generated by the midlatitude low-pressure atmospheric systems that cross the Atlantic Ocean from west to east. A thermal front develops in summer because of gradients in bottom topography and competition between surface warming induced by the solar heat flux and tidal mixing created by the bottom friction. In this frontal region, a density-driven circulation is known to interfere with the currents induced by tide and atmospheric forcing [*Le Cann*, 1982]. The evolution of the thermal structure enables trapping of nutrients in the upper ocean layers, together with phytoplankton blooms [*Videau*, 1987]. In addition, the Iroise Sea is an area of intense maritime traffic between the Atlantic Ocean and the English Channel under threat of oil spills and hazardous substance release. On account of the ecological and economical issues at stake in the Iroise Sea, a thorough knowledge of water particle displacements (also called the Lagrangian residual circulation (LRC)) according to geographic location, season, tidal, and wind conditions would prove very useful in terms of fishery and pollution management.

[3] A preliminary knowledge of the instantaneous circulation is crucial to investigations about the LRC in the Iroise Sea. From the late 1970s, many measurements (physical, chemical or biogeochemical nature of water masses, and Eulerian currents) were made in the area with moorings and fixed stations during summer cruises [*Pingree et al.*, 1975; *Mariette et al.*, 1983; *Le Corre and Mariette*, 1985]. These observations permitted the first 1-D [*Altazin-Pichon*, 1981; *Mariette*, 1983] and 2-D [*Mariette et al.*, 1982; *Mariette and Le Cann*, 1985] modeling studies. Some Lagrangian current measurements with drifting buoys were also performed on the occasion of cruises. They emphasized the density-driven circulation in the frontal areas. *Baron* [1988] used an idealized 2-D model of the instantaneous circulation in the Iroise Sea to identify Lagrangian residual structures due to tide. Numerical particles were tracked in a barycentric system of coordinates in a 2-D barotropic model that accounted only for the M2 tidal component and excluded wind forcing [*Orbi and Salomon*, 1988]. A new set of campaigns was

[1]ACTIMAR, Brest, France.
[2]Laboratoire de Physique des Océans, UMR 6523, CNRS, Ifremer, IRD, UBO, Brest, France.
[3]IFREMER, PHYSED, Plouzané, France.

0148-0227/10/2009JC005834

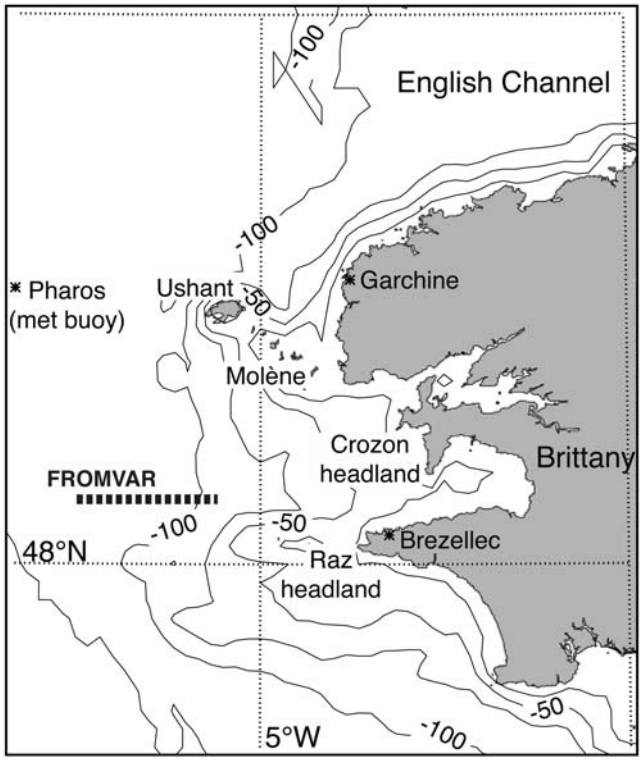

Figure 1. Shown is a map of the Iroise Sea and western end of France (Brittany) with the main geographical places used in the text and with the location of the transect made during the FROMVAR campaign in September 2007 (thick dashed line, see section 3.3). The bathymetry contour interval is 25 m.

started in summer 2005. Two coastal high-frequency (HF) radars were deployed at Brezellec and Garchine headlands to measure the sea surface currents in the area in near real time (Surveillance Littorale Opérationnelle (SURLITOP) experiment [*Mariette et al.*, 2006]) with concomitant subsurface drifters released with holey sock drogue centered at 15 m. The Variabilité du Front de Marée d'Ouessant (FROMVAR) campaign conducted in summer 2007 supplemented the previous list of measurements with conductivity-temperature-depth transects, acoustic Doppler current profiler moorings, and surface (1 m depth) and subsurface (15 m depth) Lagrangian drifter trajectories [*Le Boyer et al.*, 2009].

[4] The foreseeable nature of tide and meteorological conditions as well as the seasonal nature of the thermal front is an encouragement to study typical scenarios for the Lagrangian drift of surface water particles. Our study aims at identifying some representative situations for the surface LRC according to meteorological and oceanic conditions deduced from a 3 year data set of HF radar surface currents and from idealized modeling of the Iroise Sea. This work actually deals with the near-surface LRC since radar data account for velocity information integrated over about 25 cm [*Broche et al.*, 2003, available at www.ifremer.fr/dtmsi/colloques/see/communications] and the numerical results correspond to the first layer of a model that is about 10 cm deep in the region under radar coverage. For convenience sake, however, we chose to consider this near-surface circulation as the surface circulation.

[5] In a recent study, we introduced in detail a protocol to estimate the LRC [*Muller et al.*, 2009]. The emphasis was on methodology: we especially presented the interpolation and extrapolation of HF radar-derived surface velocity data to overcome gaps in space and time coverage. We also discussed the differences between true Lagrangian displacements and the mass transport velocity obtained with the theoretical approximation proposed by *Longuet-Higgins* [1969], and we assessed the relevance of numerical modeling for a thorough investigation of the LRC. However, for complex hydrodynamic situations such as those computed with a realistic high-resolution meteorological and oceanic modeling of the Iroise Sea, it proved very difficult to run comparison analyses between modeled surface velocity and different data sources such as drifters and HF radar-derived surface velocity. The difficulty in finding identical structures at the same place and time was an obstacle to the quantification of differences or similarities [*Muller et al.*, 2009] and showed the need to test the sensitivity of the LRC to the spatiotemporal variability of the physical processes at play. Section 2 introduces the observations and the ocean model at our disposal and presents the way we calculate the LRC. Section 3 discusses the LRC patterns derived from idealized meteorological and oceanic conditions before typical scenarios are drawn in section 4. Our conclusions follow in section 5.

2. Surface Currents

2.1. Sources of Data

[6] The joint analysis of direct observations and state-of-the-art 3-D models allows for the development of helpful Lagrangian diagnoses in the Iroise Sea [*Cambon*, 2008; *Muller et al.*, 2007]. Surface water displacements are inferred from the trajectories of numerical particles advected in a given velocity field (ocean model outputs or gridded genuine measurements issued from HF radar data) over an appropriate period of time. *Muller et al.* [2009] showed qualitative consistency between the movements of drifters released in the Iroise Sea and numerical trajectory calculations based on modeled or radar-derived sea surface velocities. They also identified the signature of different physical processes in the LRC for both origins of the gridded instantaneous surface current.

[7] To individualize the physical processes behind the LRC, we run the 3-D MARS ocean model [*Lazure and Dumas*, 2008] in idealized configurations with wind and tidal conditions extracted from typical meteorological and oceanic situations. In this way, we reproduce some specific events with calm or strong wind conditions, in neap tide or spring tide seasons and in summer or winter (see Table 1). Strong wind situations at neap tide in summer and at spring tide in winter are not presented since in both cases the residual circulation induced by the wind prevails upon the residual structures created by tide and density gradients. Our idealized modeling consists of the 667 m configuration of the Iroise Sea introduced by *Muller et al.* [2009]. The grid ranges from 5.976°W to 4.109°W and from 47.666°N to 48.831°N. The vertical resolution is based on 30 s coordinate levels that are stretched toward the surface. The tidal

Table 1. Summary of the Events Under Study and Related Model Experiments[a]

	Weak Wind Conditions						Strong Wind Conditions	
	Spring Tide			Neap Tide			Spring Tide	Neap Tide
	Summer 2005	Summer 2007	Winter	Summer 2007a	Summer 2007b	Winter	Summer	Winter
Studied events	15–18 Sep 2005	28 Sep to 1 Oct 2007	25–28 Nov 2007	5–8 Sep 2007	5–8 Sep 2007	1–4 Nov 2007	22–25 Aug 2005	10–13 Feb 2007
Wind intensity (m/s)	7	4	4.3	6	6	4.4	10	16.2
Sea level (m)	0.74–7.44	0.60–7.72	0.94–7.36	1.96–5.24	1.96–5.24	2.49–5.94	0.53–7.59	2.72–5.48
Relevant figures for studied events	4 and 6b	9	6a	14	14	3 and 7	N/A	5a
Model configuration	two-layer ocean	not modeled	homogeneous	two-layer ocean	realistic	homogeneous	two-layer ocean	homogeneous
Model tidal forcing	realistic	not modeled	realistic	realistic	realistic	realistic	realistic	realistic
Model wind forcing	Met buoy	not modeled	Met buoy	no wind	2 km winds	Met buoy	Met buoy	Met buoy
Relevant figures for model	N/A	N/A	N/A	11	15	8	N/A	5b

[a]A realistic model configuration refers to the high-resolution operational version of the MARS model forced by 2 km winds issued from a regional atmospheric model [*Muller et al.*, 2007]. A two-layer ocean refers to the model surface and bottom layers at 20°C and 13°C, respectively, with a thermocline depth located at 20 m. A homogeneous ocean refers to the full model being initialized with a 13°C temperature. Time-dependent winds from the Met buoy are applied all over the model domain without introduction of any spatial variability. A realistic tidal forcing means that the sea surface height at the model open boundaries comes from the FES 2004 [*Lyard et al.*, 2006] global tidal model with eight components (M2, S2, N2, K2, P1, O1, K1, Q1). Though the events from 28 September to 1 October 2007 and 1–4 November 2007 formally belong to autumn, they are here considered as "summer" and "winter" situations, respectively, following the corresponding homogeneous or stratified state of the ocean water column. Under neap tide conditions, a same summer event (5–8 September 2007), which appears with labels 2007a and 2007b, is studied with two different model configurations. N/A, not available.

forcing is realistic since the eight main tidal components are applied at the model open boundaries. Our representation of the Iroise Sea indeed uses a sequence of embedded 3-D configurations built on the basis of a large barotropic model, which extends from 40°N to 65°N and 20°W to 15°E with 5 km resolution. This 2-D model is forced at its open boundaries with Dirichlet-type conditions that prescribe the free surface elevation. It is computed with tidal harmonic components taken from the finite element solutions 2004 [*Lyard et al.*, 2006] (M2, S2, N2, K2, P1, O1, K1, and Q1) at 0.25° resolution and with a linear correction from the inverse barometer approximation computed from the analyzed meteorological pressure field.

[8] Hourly wind data come from the buoy Pharos located at 48.5°N, 5.6°W in the middle of the Ushant traffic separation scheme (Figure 1) and are applied all over the model sea surface without inclusion of any spatial variability. The heat fluxes at the air–sea interface are prescribed schematically in order not to complicate the interpretation of the model response to surface atmospheric forcing. The initial state of the model depends on the event under study. Winter events are simulated with a homogenous ocean at 13°C. Summer events are simulated with the 30-level model initialized as a two-layer ocean, with surface and bottom temperatures at 20°C and 13°C, respectively, and the thermocline at 20 m. The model is spun up for 2 weeks in order to have a stable thermal front when it develops. From this equilibrium, the wind time series measured at Pharos is applied, except when the focus is on horizontal thermal gradients that stand out better in simulations that dismiss wind forcing. Typical situations are selected in the Iroise Sea over this period so as to focus on specific conditions for the three physical processes under consideration: stratification, tide, and wind (see Table 1). The dates do not necessarily match those that were selected by *Muller et al.* [2009] for illustration and testing ends only and for which the Lagrangian integrations never exceeded four tidal cycles.

[9] Lagrangian integrations are also carried out with surface currents calculated by HF radars (Wellen Radar (WERA) system [*Gurgel et al.*, 1999]) whose data were regridded [*Muller et al.*, 2009]. The period considered in this study extends from August 2005 to November 2007. The spatial and temporal resolutions of the currents are 1.5 km and 12 (or sometimes 20) min, respectively. As variation in the spatiotemporal radar coverage is inevitable (because the observations are affected by changes in weather and sea state), we only consider grid points where data availability exceeds 80% of the period under study. If necessary, linear temporal and spline spatial interpolations are added to make sure that the radar coverage is constant. Therefore, the approach differs from that of *Muller et al.* [2009], who used open boundary modal analysis (OMA) to overcome spatiotemporal variations in radar range and coverage. Indeed, the OMA method requires huge computer resources in terms of memory and CPU time, which makes its use unsuitable for the systematic processing of large amount of data.

[10] Last, surface Lagrangian drifters (Technocean SVP-GPS drifters with surface Davis-type drogues at 1 m) and subsurface Lagrangian drifters (Technocean Surface Velocity Program-GPS drifters holey sock drogued at 15 m) were released over the area during the summers of 2005 and 2007 (Figure 2). When possible, we compare their original movements with the trajectories calculated with modeled or radar-derived sea surface velocities in order to strengthen the reliability of our numerical results.

2.2. Estimating the Lagrangian Residual Circulation

[11] The Lagrangian calculations were made with ARIANE, an offline diagnostic tool suitable for water mass tracing [*Blanke and Raynaud*, 1997]. The method, which is described more in detail by *Muller et al.* [2009], is the following: numerical particles are initialized at each of the U and V points of the ocean model C grid [*Arakawa and*

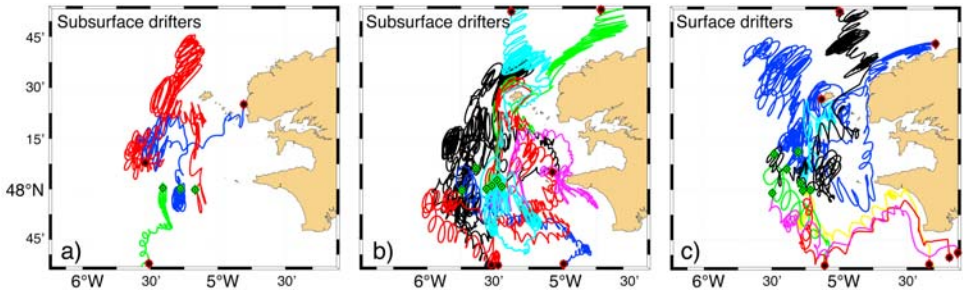

Figure 2. Trajectories of Lagrangian drifters released in summer are depicted for (a) 13 m drogued subsurface drifters in 2005, (b) 15 m drogued subsurface drifters in 2007, and (c) 1 m drogued surface drifters in 2007. In Figures 2a–2c, individual trajectories can be distinguished by their color. Initial and final positions are represented with diamonds and stars, respectively. Displacements in 2005 and 2007 are within spans from 6 September to 23 October and 6 August to 3 November, respectively.

Lamb, 1977] or at each central point of the radar grid. The trajectories are integrated over an integer number of M2 tidal cycles. The initial and final positions of each particle are used to compute a Lagrangian residual vector at the center of mass of its trajectory. Finally, the residual currents are interpolated onto the original model or radar grid. Lagrangian and Eulerian residual currents calculated with the same surface velocity field of course differ, especially nearby complex regions of bathymetry and coastline, such as west of 5°20′W, where nonlinearities are intense [*Longuet-Higgins*, 1969]. Outside these areas, differences are less noticeable though one can easily check that the Lagrangian residual currents agree better with the drifts observed with surface and subsurface drifters (Figures 3 and 4).

[12] The frequency of low- and high-pressure atmospheric systems and the slow evolution of the tidal range let us choose five M2 tidal cycles as an appropriate period of integration of the particle trajectories. This duration is sufficiently short to ensure coherent wind and tidal conditions and sufficiently long to obtain trajectories representative of the LRC. The use of a multiple of the main tidal component presupposes that the displacement measured after one M2 tidal cycle is representative of the Lagrangian residual velocity despite the involvement of several other components in the full tidal signal. The relative error on the Lagrangian residual vectors decreases with the number of M2 tidal cycles used for the Lagrangian computation though the sensitivity of the results may depend on tidal distinctive features (neap tide versus spring tide). Our Lagrangian numerical experiments are run in parallel for radar-derived and idealized modeled current data to identify typical scenarios for the surface LRC over 62 h long intervals (i.e., five M2 periods).

3. Results

[13] The velocity data sets obtained from different sources and for a varied range of hypotheses let us investigate the physical processes related to the LRC in the Iroise Sea. We study the effect of wind, tide, and density gradients in order

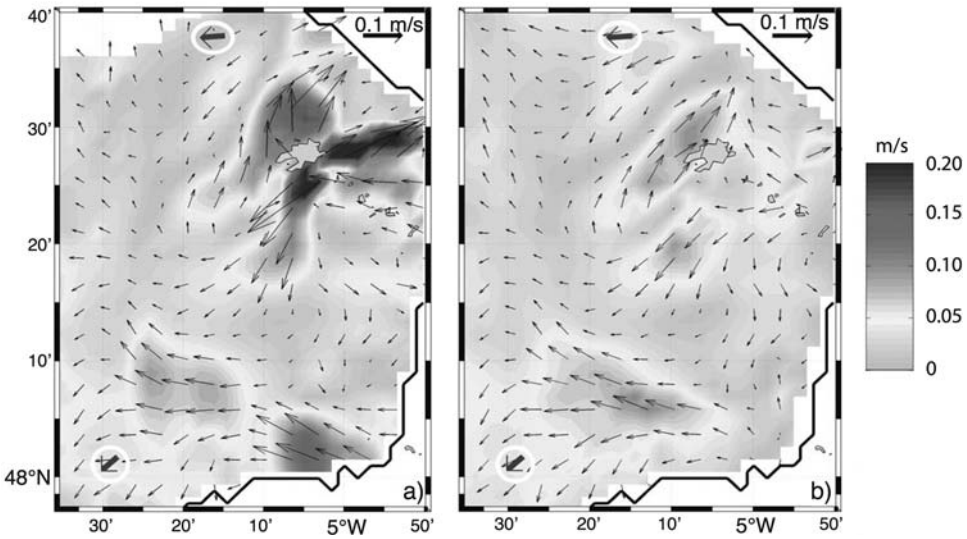

Figure 3. (a) Eulerian and (b) Lagrangian residual currents from HF radar data are shown over five tidal cycles after 1 November 2007, 0000:00 UTC, (black arrows) superimposed with the Lagrangian drift estimated from drifters (thick arrows in white circles). The shaded bar gives the magnitude of the residual current (in m/s).

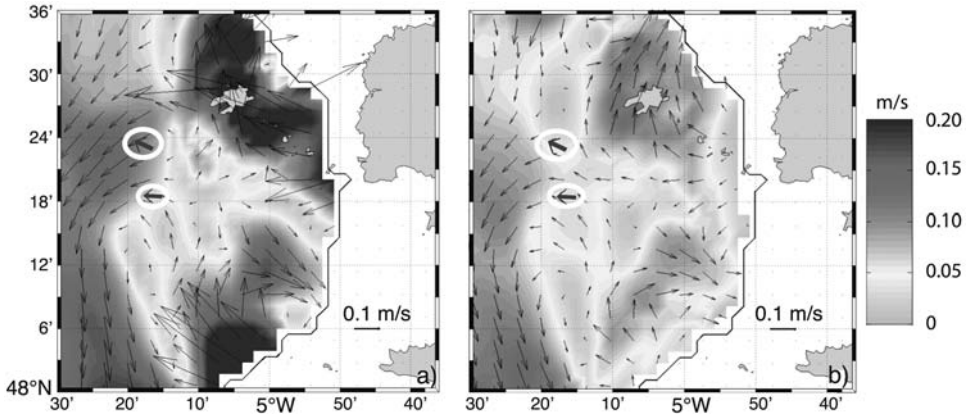

Figure 4. Same as Figure 3 except for HF radar data over five tidal cycles after 15 September 2005, 0000:00 UTC.

to get an overview of some representative scenarios of the LRC induced by various meteorological and oceanic situations.

3.1. Wind-Induced Lagrangian Residual Structures

[14] The signature of the wind on the LRC is the easiest to identify from HF radar surface currents and to simulate with an ocean model. Indeed, strong wind conditions are a prominent driving mechanism for the sea surface circulation. For the sake of simplicity, we focus on a period of neap tide, namely, the first five tidal cycles after 10 February 2007, 0000:00 UTC, during an episode of intense southwesterlies with a mean intensity of 16.2 m/s. This episode shows stronger wind conditions than around 24–26 July 2007 [*Muller et al.*, 2009], which makes it easier to study the wind as a main contributor to the LRC. The idealized modeling consists of a vertically homogeneous ocean forced by both tide and a time-dependent wind with no spatial variation (see Table 1). The resemblance and spatial homogeneity of the Lagrangian residual currents deduced from both the model and HF radar data (Figure 5) are confirmed by the same small standard deviations obtained in both cases for the zonal and meridional components: 0.04 m/s and 0.016 m/s, respectively. Moreover, the direction of the residual circulation is in agreement with results by *Jenkins* [1987], who suggested a wind-induced drift in a direction 23°–30° to the right of the wind in an ocean with depth-varying eddy viscosity coefficients. We investigated the sensitivity of the surface drift to different wind fields by calculating offshore Eulerian residual currents. Indeed, the direction of wind-induced Lagrangian residual currents is linked to the wind direction. Furthermore, the surface drift offshore is governed by the wind, and in the Iroise Sea, the difference between the Eulerian residual currents and the Lagrangian residual currents is small offshore where the nonlinearities are weak [*Muller et al.*, 2009]. Our results

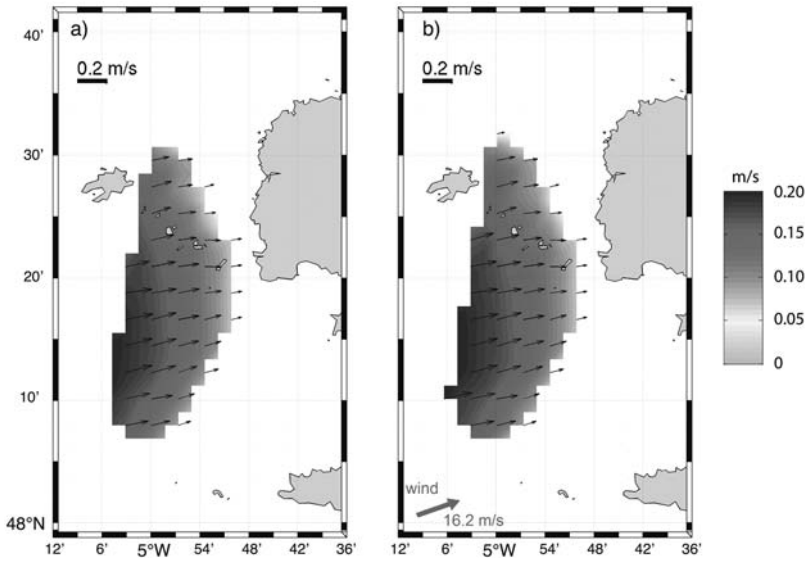

Figure 5. Lagrangian residual currents are shown over five tidal cycles after 10 February 2007, 0000:00 UTC, (black arrows) from (a) HF radar data and (b) MARS results. The shaded bar gives the magnitude of the residual current (in m/s).

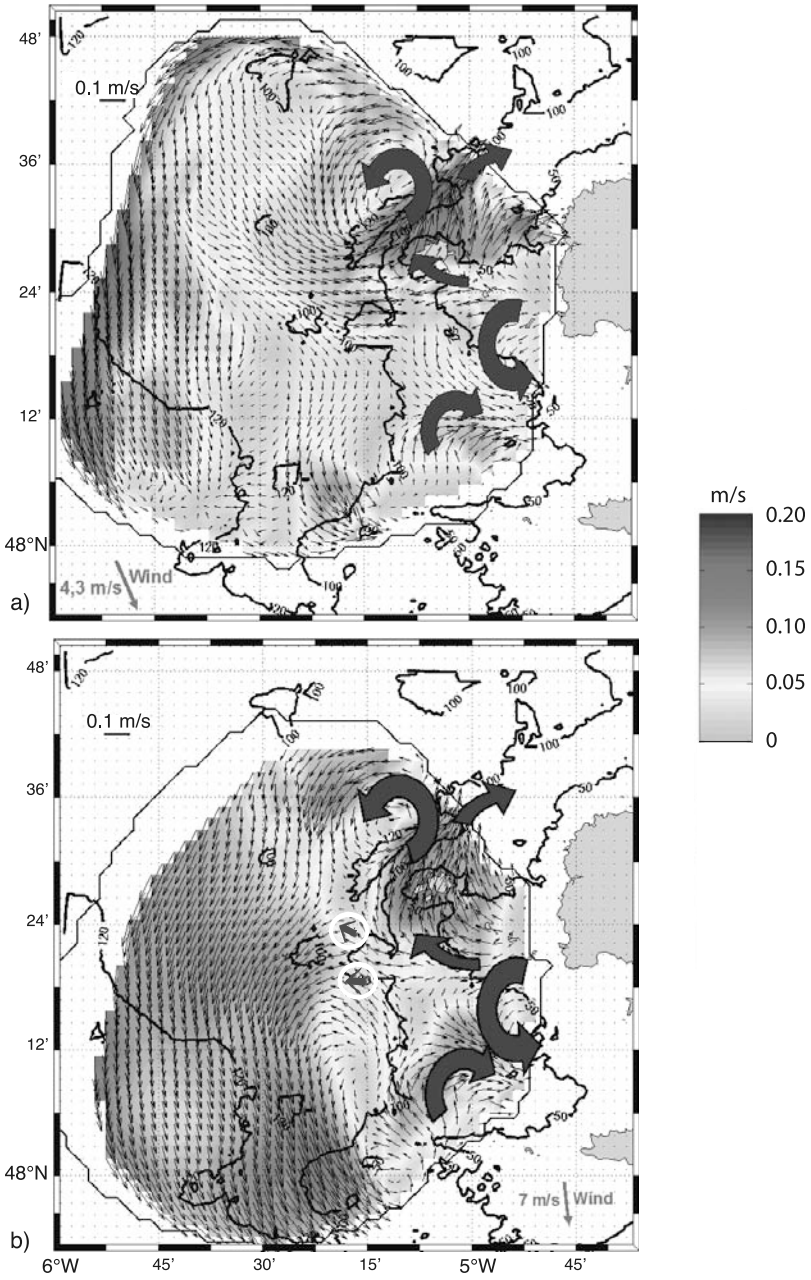

Figure 6. Lagrangian residual currents are shown from HF radar data (thin arrows) over five tidal cycles after (a) 25 November 2007, 0000:00 UTC, and (b) 15 September 2005, 0000:00 UTC. In Figure 6b the Lagrangian drift of drifters is superimposed with thick arrows in white circles. The shaded bar gives the magnitude of the residual current (in m/s). Large curved arrows identify general movements that are discussed in the text.

(not introduced here) are in agreement with the recent conclusions drawn by *Ardhuin et al.* [2009] and show that the study of Eulerian residual currents can give a satisfactory approach of Lagrangian properties offshore as long as equivalent wind conditions linger. Finally, in cases of predominantly wind-induced Lagrangian residual currents, our analysis in the Iroise Sea does not show a dependence on water depth of the angle between the wind and the wind-induced drift in accordance with the results of *Ardhuin et al.* [2009].

3.2. Tidal Lagrangian Residual Structures

[15] We focus on the following periods of spring tide and weak wind during which the tidal signal is less likely to be hidden: the first five tidal cycles after 15 September 2005, 0000:00 UTC and those after 25 November 2007, 0000:00 UTC (see Table 1). Some drifters were within the radar coverage during the summer event and are superimposed (with thick arrows) on the Lagrangian residual vectors derived from radar data to show a good coherence between both drift estimates (Figure 6). Tidal Lagrangian residual structures are

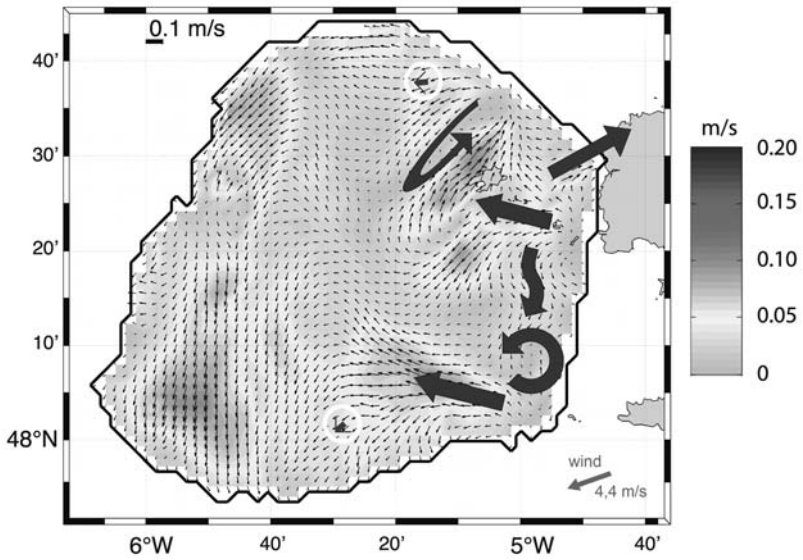

Figure 7. Lagrangian residual currents are shown from HF radar data (thin arrows) over five tidal cycles after 1 November 2007, 0000:00 UTC. The shaded bar gives the magnitude of the residual current (in m/s). Large curved arrows identify general movements that are discussed in the text. The Lagrangian drift of drifters is superimposed with thick arrows in white circles.

detectable between the coast and 5°20′W, whereas elsewhere the Lagrangian surface drift is mainly due to the wind. Within the domain of influence of tide, where tidal currents are strong and ocean depth is less than 100 m, similar patterns (large curved arrows) are identifiable in both seasons. They prevail over Lagrangian residual structures possibly induced by density gradients in summer but are likely to vanish if the wind gets stronger. Among other similarities, it is worth pointing out the residual structures found near the coast and the islands (Ushant and Molène, see Figure 1), the northern pathway north of Ushant, the cyclonic eddy to the northwest of Ushant, and the attractive line off Crozon headland (between an anticyclonic eddy off Raz headland and a cyclonic eddy nearby Molène). In order to assess the strength of such patterns whatever the season, we calculated for each component of the surface velocity field a spatial scatterplot of summer 2005 against winter 2007 velocity data, using all the grid points located between the coast and 5°20′W. We obtain a fair reproducibility of patterns between the two periods for both the zonal and meridional components of the LRC and despite the possible occurrence of spatial shifts under the influence of wind or density-driven currents. The linear correlation coefficients are 0.52 and 0.69 for the zonal and meridional current, respectively, with biases equal to −0.019 and 0.011 m/s, respectively. Tidal patterns for spring tide are easily captured by a 2-D model [*Baron*, 1988] and have already been calculated with the 3-D MARS model in the Iroise Sea [*Muller et al.*, 2009].

[16] Tide influence on residual circulation is obviously less important at neap tide than at spring tide; it is even uneasy to clearly identify its influence during weak wind conditions. Here we study a winter situation characterized by northeasterly winds of about 4.4 m/s and corresponding to the five tidal cycles following 1 November 2007, 0000:00 UTC (Figures 7 and 8). Again, the superimposition of Lagrangian displacements of drifters gives credit to the LRC calculations. The structure of the residual circulation bears some resemblance with the one derived during spring tide (Figure 6), with a cyclonic eddy to the northwest of Ushant and a northwestward circulation to the south of Molène. The idealized modeling is able to capture some elements of the residual circulation (Figure 8), except outside the domain of influence of tide where wind is prevailing and near the coast where radar data are less reliable [*Muller et al.*, 2007]. The model is rather successful in retrieving the zonal component of the residual circulation (as deduced from radar data). A scatterplot of model against radar-derived data gives a 0.94 linear correlation coefficient over the area under study (delimited by the black contours on Figures 7 and 8). However, the model is far less satisfactory for the meridional component (0.21 correlation coefficient). The latter poor correlation can be partly explained by the presence of a strong northward drift near Molène in the idealized model. Both the lack of reliable radar data in this area and the restrictions of the modeling approach induced by carrying out idealized configurations cast doubt on this northward circulation. A more realistic result would have been obtained with high-resolution winds in order to account for variations of wind direction between the northern and eastern areas of the domain and, hence, to calculate a better residual circulation nearby Molène island. Yet this study shows that whatever the season, weak wind conditions are favorable to typical tide-induced features in the LRC in agreement with the idealized 2-D modeling carried out by *Baron* [1988]. Additional diagnoses (not shown) show that nearby the coast, where nonlinearities are strong, the residual circulation at spring tide can be 10 times more intense than at neap tide.

3.3. Residual Structures Induced by Density Gradients

[17] Lagrangian residual structures induced by density gradients can be observed only under calm weather conditions. Sea surface temperature (SST) may be used to reveal

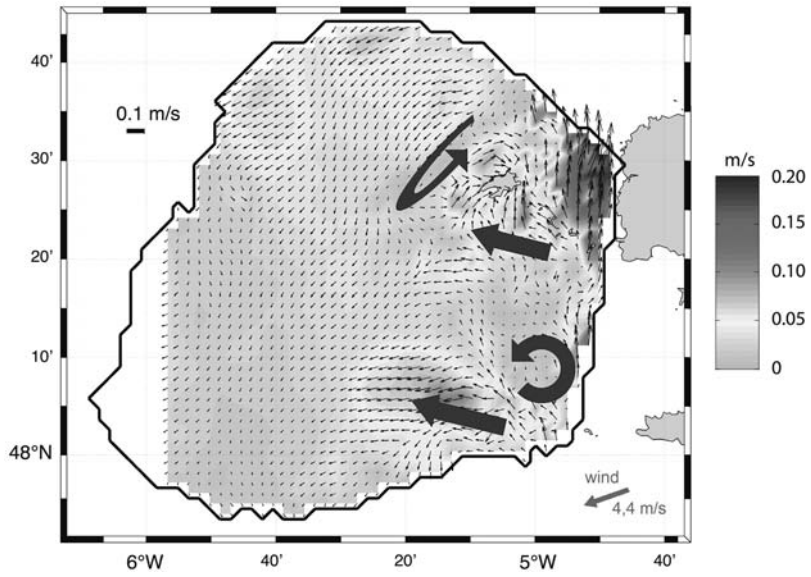

Figure 8. Same as Figure 7 except for MARS results.

such events since in the Iroise Sea, density-driven currents are mainly due to thermal gradients and, consequently, develop preferentially in the thermal front region [*Le Boyer et al.*, 2009]. The superimposition of the Lagrangian residual currents deduced from HF radar data over the five tidal cycles following 28 September 2007, 0000:00 UTC (spring tide conditions, see Table 1), and the satellite SST recorded on 28 September 2007, 0200:00 UTC, highlights an along-front drift (Figure 9). Its direction can be explained by the vertical structure of temperature and the thermal wind equations. The transect made, at the same period, during the FROMVAR experiment [*Le Boyer et al.*, 2009] indeed shows some horizontal distance between the surface and bottom thermal fronts (Figure 10). This leads to a southward along-front drift velocity and a northward current in the stratified region and in the homogeneous region, respectively [*Le Boyer et al.*, 2009]. Cross-frontal mixing is confirmed by frontal instabilities and by the development of cyclonic eddies (about 20–40 km in diameter and 3–4 days in lifetime) in the frontal area [*Pingree*, 1978]. Small

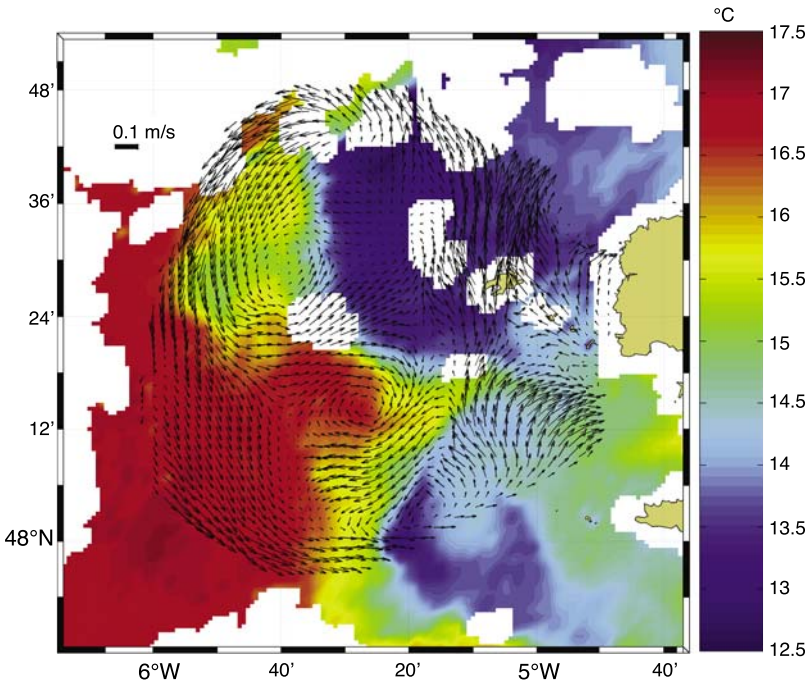

Figure 9. Lagrangian residual currents are shown from HF radar data over five tidal cycles after 28 September 2007, 0000:00 UTC, (thin arrows) and satellite SST on 28 September 2007, 0200:00 UTC (in color). The color bar gives the value of the SST (in °C).

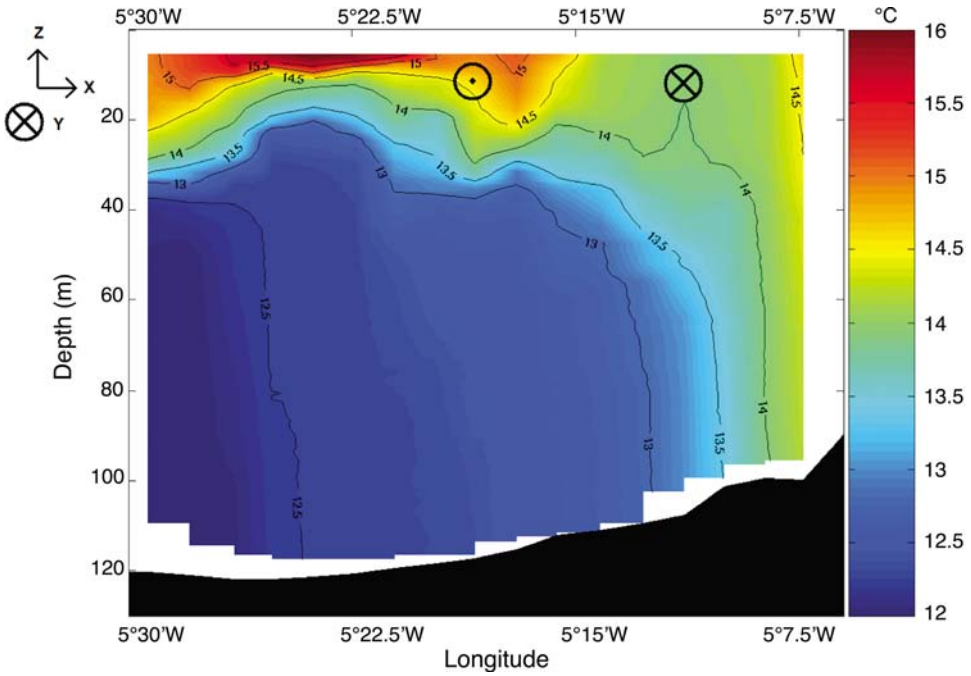

Figure 10. Vertical temperature structure (in color and with contours) across the Iroise Sea at 48.15°N measured during the FROMVAR campaign (September 2007, see Figure 1) and orientation of the density-driven currents calculated with the thermal wind equations. The color bar gives the value of the temperature (in °C).

meanders can also appear on SST [*Pingree*, 1978], as well as anticyclonic eddies depending on the orientation of the front; however, these are fewer in number than cyclones [*Pingree*, 1978; *Le Boyer et al.*, 2009].

[18] An idealized modeling with a two-layer ocean forced by tide and without wind (see Table 1) reproduces the density-driven circulation together with its associated cyclonic eddies. The 17°C isotherm is here chosen as a proxy for the thermal front and is superimposed on the LRC modeled over the five tidal cycles following 5 September 2007, 0000:00 UTC (Figure 11). An anticyclonic eddy circulation stands out at 48°09′N, where the front is the closest

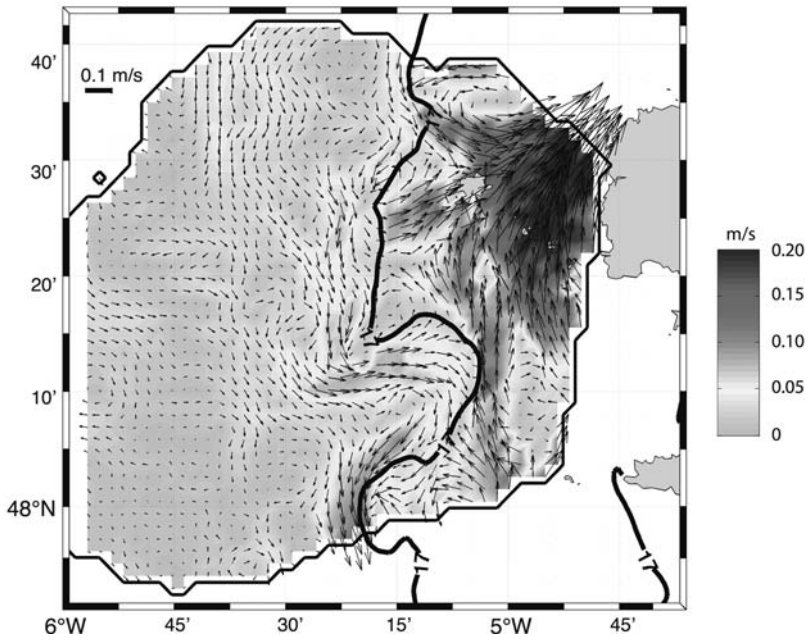

Figure 11. Lagrangian residual currents are shown from MARS results over five tidal cycles after 5 September 2007, 0000:00 UTC (thin arrows), superimposed with the isotherm 17°C (thick line). The shaded bar gives the magnitude of the residual current (in m/s).

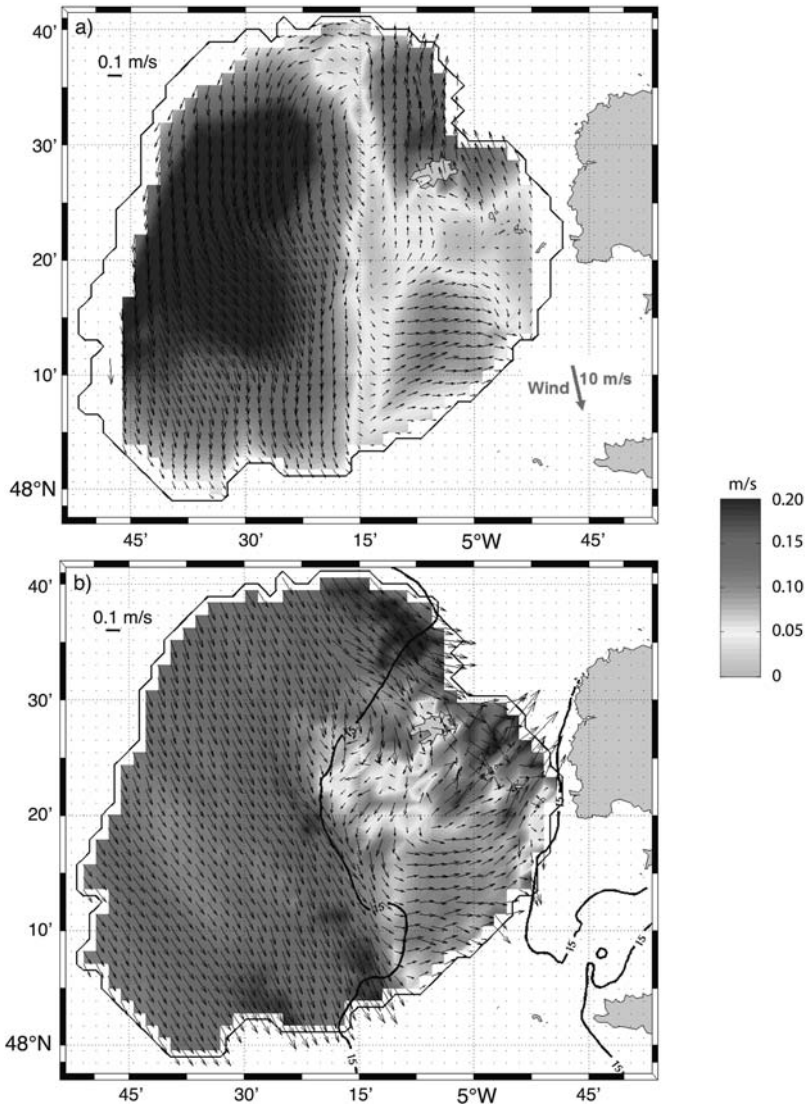

Figure 12. Lagrangian residual currents are shown over five tidal cycles after 22 August 2005, 0000:00 UTC, from (a) HF radar data and (b) MARS results (black line is the superimposition of the 15°C isotherm).

to the coastline. The modeling results agree fairly well with the LRC deduced from radar data (Figure 9) even though the idealized model is not run here over the same tidal conditions. The intensity of the density-driven drift is, for instance, of the same order of magnitude (about 7 cm/s) and shows the ability of the ocean model to reproduce this particular and seasonal physical process.

[19] The cyclonic circulation at the mouth of the English Channel (Figure 11) recalls that observed with drifters by *Pingree et al.* [1999] or reproduced by 2-D modeling [*Salomon and Breton*, 1993; *Bailly du Bois and Dumas*, 2005]. It is worth noting that the modeling experiments that show this circulation do not necessarily take the wind into account, and simple 2-D barotropic models can reproduce it, which means that it is tide generated. At the present stage of our analysis, it is difficult to establish whether the density-driven flow identified in our study is linked only to the thermal front (which would be our first guess) or if it is also related to this cyclonic circulation identified with tidal models at the mouth of the English Channel.

[20] The identification of residual structures related to the thermal front is easy only when weak winds prevail with concomitant spring tide conditions. Indeed, at spring tide, tidal currents are stronger and induce a vertical mixing more efficient than at neap tide. As a result, thermal gradients between the open ocean and coastal areas are stronger, which implies more intense density-driven currents. Moreover, the stratified area is closer to the coast at neap tide, and so is the thermal front. Therefore, the tidal front position also oscillates with the spring tide/neap tide cycle. The density-driven currents and associated eddies are no longer noticeable with a northwesterly average wind of about 10 m/s during the five tidal cycles following 22 August 2005, 0000:00 UTC (Figure 12). However, the residual currents calculated with either radar data or idealized modeling show a slowdown of the LRC, in the frontal area, caused by the

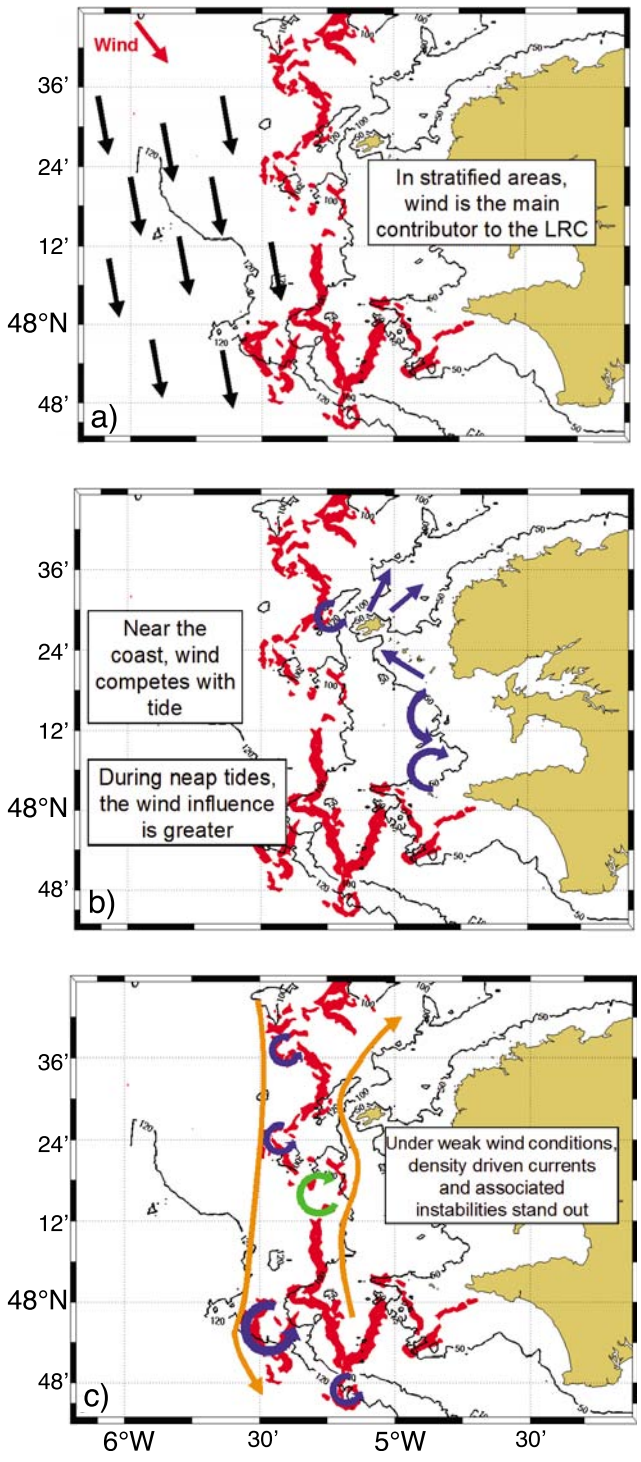

Figure 13. Typical scenarios for the LRC in the Iroise Sea impact of (a) wind, (b) tide, and (c) thermal gradients. The thermal front (in red) is deduced from the remote sensing of SST on 8 August 2007. Thick dark arrows (in black, blue, or green) identify prominent features of the LRC that are discussed in the text. Orange arrows in Figure 13c show the general orientation of the density-driven currents.

added influence of wind- and density-driven currents. Indeed, while density-driven along-front currents have opposite directions on both sides of the thermal front, the wind-driven circulation generates southeastward surface currents that accelerate and decelerate the circulation, west and east of the front, respectively.

[21] This conclusion cannot be drawn for stronger winds (>10 m/s) or medium winds whose direction is perpendicular to the direction of the density-driven currents. In such cases, the wind governs the surface LRC all over the area and the wind-induced drift prevails over the density-driven residual circulation. The surface LRC due to density gradients is noticeable during weak wind conditions or during north–south wind conditions that reinforce the density-driven circulation on one side of the thermal front and decelerate it on the other side.

4. Discussion

[22] Real-time hydrodynamic simulations run with high-resolution meteorological and oceanic models can be hard to compare with trajectories of drifters and HF radar-derived surface velocity, especially because small-scale structures may not be found at the same place and time [*Muller et al.*, 2009]. This new study provides answers to this issue by mapping the LRC in the Iroise Sea for specific weather, tidal, and density gradient conditions over periods equal to five cycles of the predominant tidal wave (M2). The ocean model was run over idealized situations in order to reduce the degree of complexity of the analysis. These situations were selected so as to span the most typical meteorological and oceanographic conditions encountered in the Iroise Sea. The main strength of the approach is the ability to switch on and off individual physical processes in the model in order to isolate in the LRC the patterns induced by the atmospheric forcing, tides, and density-driven currents.

[23] The Lagrangian interpretation proves successful in retrieving residual structures induced by wind and tide. These driving mechanisms produce Lagrangian currents more pronounced than the residual circulation induced by density gradients and therefore lead to dynamic situations that are more likely predictable. The mapping of typical scenarios for the Lagrangian residual currents marks a substantial advance in the knowledge of the dynamics in the Iroise Sea. It is here worth noting that the ocean model has still some difficulty in reproducing the thermal front at its exact position [*Muller et al.*, 2007], which would have pessimistic implications for an operational reproduction of the LRC. Fortunately, in the Iroise Sea, the contribution of density-driven currents to the LRC appears to be significant only under the conditions of weak or northerly winds. Medium southerly winds may have the same impact as northerly winds on the persistence of the density-driven residual structures, but such situations were not recorded in our data sets.

[24] The analysis of typical samples of the LRC over five tidal cycles and under given meteorological and oceanic conditions permits the classification of representative scenarios (Figure 13). In Figure 13, the thermal front (drawn in red) is deduced from the remote sensing of SST on 8 August 2007 so as to reproduce all its small scales [*Muller et al.*, 2009]. Blue arrows schematize the LRC derived from our

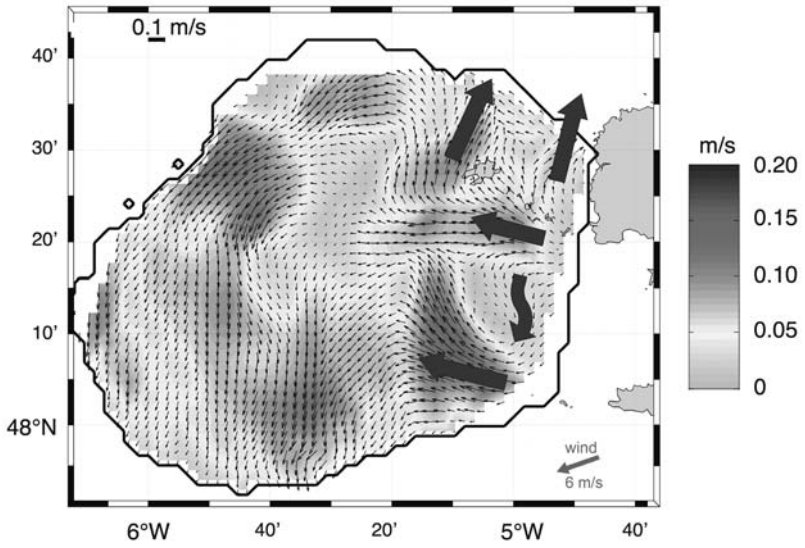

Figure 14. Lagrangian residual currents are shown from HF radar data (thin arrows) over five tidal cycles after 5 September 2007, 0000:00 UTC. The shaded bar gives the magnitude of the residual current (in m/s). Large curved arrows identify general movements that are discussed in the text.

analysis. In summer, when the tidal thermal front is present, wind prevails offshore over all the other physical processes. The wind-induced drift slightly veered to the right of the wind direction (Figure 13a, for northwesterly wind conditions). Near the coast, wind and tide compete though the effect of the wind dominates during neap tides (Figure 13b). Under weak wind conditions, density-driven currents and related instabilities can stand out (Figure 13c).

[25] The identification of robust patterns in the Iroise Sea, from both radar-derived data and idealized modeled currents, encourages the use of a high-resolution, realistic meteorological, and oceanic model to reproduce and test them. The details of such a state-of-the-art modeling approach are given by *Muller et al.* [2007]. Here a preliminary Lagrangian analysis is performed over the five tidal cycles following 5 September 2007, 0000:00 UTC, both for radar-derived surface currents (Figure 14) and for the regional model (Figure 15). Some similarities arise from the inspection of the LRC maps, even though obvious differences between the two fields, especially in frontal areas, are indicative of the inability of the ocean model to reproduce the density-driven circulation at the right times and places.

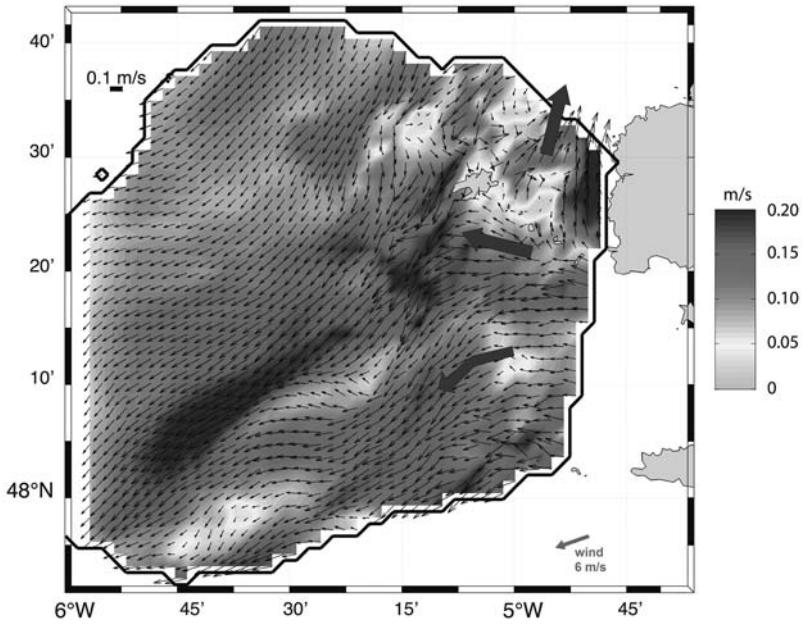

Figure 15. Same as Figure 14 except for currents from the high-resolution, realistic configuration of the MARS model.

Other discrepancies concern the intensity of the wind-induced Lagrangian residual currents that is generally larger in the high-resolution model than in the radar-derived surface circulation. They may stem from an overestimation of the wind stress, notably through an imperfect optimization of the drag coefficient used at the sea surface. The operational version of the MARS 3-D code currently uses the quadratic parameterization proposed by *Geernaert and Katsaros* [1986] for surface friction: $C_d = 0.001 \times (0.43 + 0.097 \times \text{wind speed})$. A drag coefficient linked to the surface roughness and SST could likely be more relevant in future process studies of the Iroise Sea.

5. Concluding Remarks

[26] We used three complementary approaches to study the Lagrangian residual circulation in the Iroise Sea: (1) the trajectories followed by several drifters released in the area; the Lagrangian residual currents deduced from the trajectory analysis of numerical particle moving within either (2) HF radar-derived or (3) modeled surface currents. Thanks to the 3 year coverage of the HF radar data set and to a regional ocean model run in idealized configurations, we identified typical scenarios for the LRC calculated over 2.5 day periods, depending on concomitant meteorological and oceanic conditions and distinguishing the effect of wind forcing, tide, and density gradients.

[27] The analysis of the LRC over these scenarios for both idealized modeling and radar-derived data suggests a tendency of the model to reproduce better the signature of wind and tide than the effect of density-driven currents. Our attempt to mimic the observed LRC with a realistic, operational model configuration highlighted some problems; slight discrepancies in the modeled Eulerian velocities can lead to significant errors on computed trajectories of water particles. Improving the instantaneous velocity field computed by the operational version of the MARS 3-D model is our first priority. Ongoing investigation focuses on an improved drag coefficient parameterization at the sea surface and on a better calibration of the vertical turbulent closure scheme. Indeed, our analysis of the signature of the different physical processes at play in the LRC suggests possibly a biased estimation of the vertical mixing intensity. Thus, further investigation is needed to build an operational tool for drift prediction in the Iroise Sea. In the case of environmental accidents such as the oil spills by tankers Erika (1999, 30,000 tons) and Amoco-Cadiz (1978, 223,000 tons), the availability of a model capable of reproducing accurately such processes would be of great help for decision makers.

[28] **Acknowledgments.** We thank two anonymous reviewers and the Editor for helpful and detailed comments. We acknowledge the ACTIMAR firm for its financial support. We are grateful to SHOM (the French naval hydrographic and oceanographic service) and ACTIMAR for putting at our disposal the high-frequency radar data collected within the SURLITOP project (initiated by the RITMER network and the VIGICOTE project). The SST data have been produced by SAF (Satellite Application Facility) of EUMETSTAT/Météo-France and provided through the CERSAT satellite image browser facility. We also acknowledge Météo-France for making available data from the meteorological stations located in the Iroise Sea, under an agreement between Météo-France and the Université de Bretagne Occidentale (UBO). We thank also Louis Marié for giving us some preliminary results of the FROMVAR sea experiment conducted in summer 2007.

References

Altazin-Pichon, A. (1981), Application d'un modèle de thermocline à la formation du front thermique en mer d'Iroise. Confrontation des résultats avec des mesures in situ, Ph.D. thesis, 140 pp., Univ. de Bretagne Occident., Brest, France.

Arakawa, A., and V. R. Lamb (1977), Computational design of the basic dynamical process of the UCLA general circulation model, in *General Circulation Models of the Atmosphere*, *Methods Comput. Phys.*, vol. 17, edited by J. Chang, pp. 173–265, Academic, New York.

Ardhuin, F., L. Marié, N. Rascle, P. Forget, and A. Roland (2009), Observation and estimation of Lagrangian, Stokes, and Eulerian currents induced by wind and waves at the sea surface, *J. Phys. Oceanogr.*, *39*, 2820–2838, doi:10.1175/2009JPO4169.1.

Bailly du Bois, P., and F. Dumas (2005), Fast hydrodynamic model for medium- and long-term dispersion in seawater in the English Channel and southern North Sea, qualitative and quantitative validation by radionuclide tracers, *Ocean Modell.*, *9*, 169–210, doi:10.1016/j.ocemod.2004.07.004.

Baron, Y. (1988), A Lagrangian model for long-term tidally induced transport and mixing. Verification by artificial radionuclide concentrations, in *Radionuclides: A Tool for Oceanography*, edited by J. C. Guary, P. Guéguéniat, and R. J. Pentreath, pp. 384–394, Elsevier Appl. Sci., London.

Blanke, B., and S. Raynaud (1997), Kinematics of the Pacific Equatorial Undercurrent: An Eulerian and Lagrangian approach from GCM results, *J. Phys. Oceanogr.*, *27*, 1038–1053, doi:10.1175/1520-0485(1997)027<1038:KOTPEU>2.0.CO;2.

Broche, P., P. Forget, J.-C. de Maistre, Y. Barbin, and J. Gaggelli (2003), VHF radars for remote sensing of the surface coastal currents, paper presented at SEE Workshop on Radar and Marine Environment, Ifremer, Brest, France, 10 June.

Cambon, G. (2008), Étude numérique de la mer d'Iroise: Dynamique, variabilité du front d'Ouessant et évaluation des échanges cross-frontaux, Ph.D. thesis, Univ. de Bretagne Occident., Brest, France.

Geernaert, G. L., and K. B. Katsaros (1986), Incorporation of stratification effects on the oceanic roughness length in the derivation of the neutral drag coefficient, *J. Phys. Oceanogr.*, *16*, 1580–1584, doi:10.1175/1520-0485(1986)016<1580:IOSEOT>2.0.CO;2.

Gurgel, K.-W., G. Antonischki, H.-H. Essen, and T. Schlick (1999), Wellen Radar (WERA): A new ground-wave HF radar for ocean remote sensing, *Coastal Eng.*, *37*, 219–234, doi:10.1016/S0378-3839(99)00027-7.

Jenkins, A. D. (1987), Wind and wave induced currents in a rotating sea with depth-varying eddy viscosity, *J. Phys. Oceanogr.*, *17*, 938–951, doi:10.1175/1520-0485(1987)017<0938:WAWICI>2.0.CO;2.

Lazure, P., and F. Dumas (2008), An external-internal mode coupling for a 3D hydrodynamical model for applications at regional scale (MARS), *Adv. Water Resour.*, *31*, 233–250, doi:10.1016/j.advwatres.2007.06.010.

Le Boyer, A., G. Cambon, N. Daniault, S. Herbette, B. Le Cann, L. Marié, and P. Morin (2009), Observations of the Ushant tidal front in September 2007, *Cont. Shelf Res.*, *29*, 1026–1037, doi:10.1016/j.csr.2008.12.020.

Le Cann, B. (1982), Évolution annuelle de la structure hydrologique du plateau continental au Sud de la Bretagne. Modélisation numérique, Ph.D. thesis, 251 pp., Univ. de Bretagne Occident., Brest, France.

Le Corre, P., and V. Mariette (1985), Le front thermique d'Ouessant en août et Septembre 1982, campagne Satir Dynatlant. *Campagne Océanogr. Fr. 1-1985*, 369 pp., Ifremer, Brest, France.

Le Duff, M., and C. Hily (1999), L'environnement Naturel de l'Iroise-Bilan des connaissances et Intérêt Patrimonial-Septembre 1999, vol. 2, 83 pp., Univ. de Bretagne Occident., Brest, France.

Longuet-Higgins, M. S. (1969), On the transport of mass by time-varying ocean currents, *Deep Sea Res. Oceanogr. Abstr.*, *16*, 431–447, doi:10.1016/0011-7471(69)90031-X.

Lyard, F., F. Lefèvre, T. Letellier, and O. Francis (2006), Modelling the global ocean tides: Modern insights from FES 2004, *Ocean Dyn.*, *56*, 394–415, doi:10.1007/s10236-006-0086-x.

Mariette, V. (1983), Effet des échanges atmosphériques sur la structure thermique marine. Application à des zones du large et à une zone côtière, Ph.D. thesis, 282 pp., Univ. de Bretagne Occident., Brest, France.

Mariette, V., and B. Le Cann (1985), Simulation of the formation of Ushant thermal front, *Cont. Shelf Res.*, *4*, 637–660, doi:10.1016/0278-4343(85)90034-2.

Mariette, V., G. Rougier, J. C. Salomon, and B. Simon (1982), Courants de marée en Mer d'Iroise, *Oceanol. Acta*, *5*, 149–159.

Mariette, V., J.-P. Le Saos, and G. Rougier (1983), Résultats des mesures d'océanographie physique réalisées lors de la campagne Satir Dynatlant,

scientific report, 110 pp., Lab. d'Océanogr. Phys., Univ. de Bretagne Occident., Brest, France.
Mariette, V., N. Thomas, V. Cochin, Y. Guichoux, and F. Ardhuin (2006), Premiers résultats de l'expérience SURLITOP (Surveillance Littorale Opérationnelle), *Navigation*, *54*, 45–57.
Muller, H., F. Dumas, B. Blanke, and V. Mariette (2007), High-resolution atmospheric forcing for regional oceanic model: The Iroise Sea, *Ocean Dyn.*, *57*, 375–400, doi:10.1007/s10236-007-0115-4.
Muller, H., F. Dumas, B. Blanke, and V. Mariette (2009), Estimating the Lagrangian residual circulation in the Iroise Sea, *J. Mar. Syst.*, *78*, suppl. 1, S17–S36, doi:10.1016/j.jmarsys.2009.01.008.
Orbi, A., and J.-C. Salomon (1988), Dynamique de marée dans le Golfe Normand-Breton, *Oceanol. Acta*, *11*, 55–64.
Pingree, R. D. (1978), Cyclonic eddies and cross-frontal mixing, *J. Mar. Biol. Assoc. U. K.*, *58*, 955–963, doi:10.1017/S0025315400056885.
Pingree, R. D., P. R. Pugh, M. Holligan, and G. R. Forster (1975), Summer phytoplankton blooms and red tides along tidal fronts in the approaches to the English Channel, *Nature*, *258*, 672–677, doi:10.1038/258672a0.
Pingree, R. D., B. Sinha, and C. R. Griffiths (1999), Seasonality of the European slope current (Goban Spur) and ocean margin exchange, *Cont. Shelf Res.*, *19*, 929–975, doi:10.1016/S0278-4343(98)00116-2.
Salomon, J.-C., and M. Breton (1993), An atlas of long-term currents in the Channel, *Oceanol. Acta*, *16*, 439–448.
Videau, C. (1987), Primary production and physiological state of phytoplankton at the Ushant tidal front (west coast of Brittany, France), *Mar. Ecol. Prog. Ser.*, *35*, 141–151, doi:10.3354/meps035141.

B. Blanke, Laboratoire de Physique des Océans, UMR 6523, CNRS, Ifremer, IRD, UBO, 6 ave. Le Gorgeu, F-29238 Brest, France. (blanke@univ-brest.fr)
F. Dumas, Ifremer, PHYSED, B.P.70, F-29280 Plouzané, France.
V. Mariette and H. Muller, ACTIMAR, 24 quai de la Douane, F-29200 Brest, France.